

Electrical Excitation of Surface Plasmons

Palash Bharadwaj,¹ Alexandre Bouhelier,² and Lukas Novotny^{1,*}

¹*Institute of Optics and Department of Physics and Astronomy, University of Rochester, Rochester, New York 14627, USA*

²*Laboratoire Interdisciplinaire Carnot de Bourgogne, CNRS UMR-5209, Université de Bourgogne, 21000 Dijon, France*

(Received 1 November 2010; revised manuscript received 7 May 2011; published 2 June 2011)

We exploit a plasmon mediated two-step momentum down-conversion scheme to convert low-energy tunneling electrons into propagating photons. Surface plasmon polaritons (SPPs) propagating along an extended gold nanowire are excited on one end by low-energy electron tunneling and are then converted to free-propagating photons at the other end. The separation of excitation and outcoupling proves that tunneling electrons excite gap plasmons that subsequently couple to propagating plasmons. Our work shows that electron tunneling provides a nonoptical, voltage-controlled, and low-energy pathway for launching SPPs in nanostructures, such as plasmonic waveguides.

DOI: 10.1103/PhysRevLett.106.226802

PACS numbers: 73.20.Mf, 68.37.Ef, 73.40.Gk, 78.68.+m

The momentum of a nonrelativistic free electron of mass m_e is a factor $\sqrt{2m_e c^2 / \hbar \omega} \sim 500$ greater than that of a visible photon of the same energy. This implies that the interaction between electrons and photons is weak for $\hbar \omega \ll m_e c^2$, since energy and momentum cannot be simultaneously conserved. One way to bridge this mismatch is to employ polariton modes (plasmons). They have the same energy as free space photons but arbitrarily high spatial localization (hence momentum), and can therefore couple efficiently to electrons [1].

The idea to use electrons to excite surface plasmon polaritons (SPPs) in metals dates back to Ritchie's landmark paper of 1957 [2]. High-energy (~ 30 keV) free electrons have since been used to excite both propagating [3–5] and localized plasmons [6,7]. A novel low-energy route based on inelastic electron tunneling was discovered by Lambe and McCarthy in experiments with roughened metal-insulator-metal junctions [8], ultimately leading to the observation of light emission from the scanning tunneling microscope (STM) [9,10]. The origin of STM photoemission lies in the highly localized gap plasmons excited in the tip-sample cavity by inelastically tunneling electrons [11,12]. Early experiments suggested that gap plasmons could in turn excite extended surface plasmons (SPPs), which can decay radiatively in a glass substrate [13–15]. Although advances in the field of STM have enabled the control of photoemission on the atomic scale [16–19], the excitation of extended plasmonic structures by tunneling electrons has not yet been addressed. So far, electrical SPP excitation schemes employed either high-energy electrons [3–5] or near-field coupling of electro-luminescent excitons [20,21].

In this Letter we demonstrate a direct energy conversion route from electrons to photons, accomplished via intermediate plasmonic excitations. Specifically, we employ inelastic electron tunneling to excite localized gap plasmons in the junction of a gold tip and a monocrystalline gold nanorod. The gap plasmons then couple to

propagating SPPs, which in turn are converted to propagating photons by edge scattering. The experimental configuration, shown in Fig. 1, is a combination of an inverted optical microscope and a STM.

A bias voltage is applied between the sample and a gold tip, whose position is held under feedback at a constant tunneling current. Light is collected on the substrate side with a high numerical aperture (NA = 1.4) objective, and the full angular distribution of emitted photons is recorded by imaging the back focal plane (Fourier plane) of the objective on an electron-multiplying charge-coupled device camera. Alternatively, the distribution of photons in real space can be mapped by including another focusing lens in the imaging path.

To characterize the electron-photon coupling mechanism we first investigated the electrical excitation of extended propagating SPPs on a thermally evaporated Au

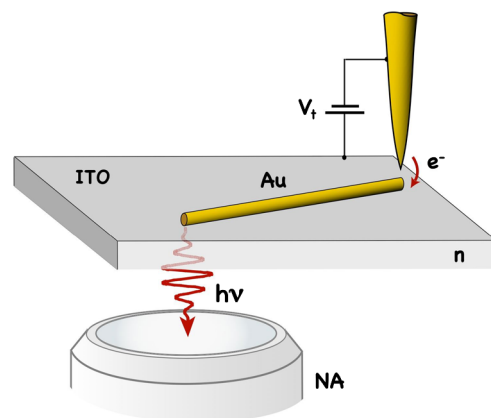


FIG. 1 (color online). Illustration of the experiment. Inelastic electron tunneling between a gold tip and a single-crystal gold nanorod gives rise to surface plasmon excitation. Locally excited surface plasmons propagate along the nanorod and scatter at the other end. Emitted photons are collected by an index-matched NA = 1.4 objective and then analyzed.

film deposited on a glass substrate ($n = 1.52$). A film thickness of 20 nm provides a compromise between SPP propagation length and film transparency for detection of leakage radiation. A chemically etched ~ 50 nm sharp Au tip was brought in tunneling contact to the surface (typical substrate bias $V_t = 2$ V; tunneling current $I_t = 1$ nA; tip-sample distance ~ 9 Å), giving rise to a photon count rate of 5–10 kc/s, which corresponds to an electron-photon conversion efficiency of $\sim 10^{-5}$. For biases of 1.9 V and higher, the spectrum of the emitted light spans from 650 to 800 nm, peaking around 700 nm [22]. The exact spectral profile depends on the tip shape [23]. For a 20 nm gold film and a free space wavelength of $\lambda = 700$ nm, the SPP has a wave vector of $k_{\text{SPP}} = 1.06k_0$, where $k_0 = 2\pi/\lambda$ is the free space wave vector. Because of the finite film thickness and the supporting glass substrate, the excited SPPs decay via leakage radiation that is emitted into the Kretschmann angle at $\theta_K = 43.8^\circ$.

To experimentally verify the electrical excitation of SPPs and their radiative decay, we imaged the intensity distribution of the emitted photons in the back focal plane of the collection objective. The recorded intensity map can be directly translated into an angular radiation pattern or a momentum distribution of the emitted photons. As shown in Figs. 2(a) and 2(b), the intensity distribution is rotationally symmetric and features a ring whose radius

corresponds to an emission angle of $\theta \approx 44^\circ$. This angle is larger than the critical angle of total internal reflection $\theta_c = \arcsin[1/n] \approx 41.1^\circ$ and is readily identified as the Kretschmann angle. We find that more than $\sim 90\%$ of the total radiation is emitted at angles larger than θ_c . To analyze the spatial polarization distribution of the emitted radiation, we place a polarizer behind the back focal plane of the objective. The resulting intensity distribution is shown in the inset of Fig. 2(a) for one particular polarizer orientation. The photons in the ring are almost p polarized, as expected for leakage radiation from propagating surface plasmons. The incomplete extinction is likely due to scattering of localized gap modes from surface roughness.

In a next step we replaced the 20 nm gold film by a ~ 5 nm granular gold film, which does *not* support propagating SPPs. As expected, gap plasmons excited by inelastic electron tunneling are not able to couple to SPPs and hence no plasmon ring could be observed. Instead, the back focal plane image features a uniform intensity pattern with a discontinuity at θ_c , suggesting that the light originates from a localized but randomly oriented source distribution [24].

The physical mechanism behind electron-excited SPP generation can be described by a two-step process. Inelastically tunneling electrons first couple to localized modes of the tip-sample junction (gap plasmons). The excited gap plasmons then couple to SPPs propagating along the gold-air interface. The excited gap plasmons can be represented by an oscillating vertical dipole \mathbf{p}_z . In terms of the transmission coefficient $t^{(p)}$ of the gold film, the in-plane momentum (k_{\parallel}) distribution of transmitted photons can be calculated as [25]

$$\hat{\mathbf{E}}(k_{\parallel}) = \frac{ip_z}{8\pi^2\epsilon_0} \frac{k_{\parallel} t^{(p)}(k_{\parallel})}{\sqrt{1 - k_{\parallel}^2/k_0^2}} \exp[ik_0 z_0 \sqrt{1 - k_{\parallel}^2/k_0^2}] \mathbf{n}_\rho, \quad (1)$$

where z_0 is the height of the dipole above the gold surface and \mathbf{n}_ρ is the unit vector in radial direction parallel to the gold layer. The intensity in the back focal plane corresponds to the modulus square of $\hat{\mathbf{E}}(k_{\parallel})$. The numerical aperture of the collection objective restricts the range of spatial frequencies to $k_{\parallel} = [0 \dots k_0 \text{NA}]$. The angle θ used for the cross sections in Fig. 2 is related to k_{\parallel} by $\sin[k_{\parallel}] = \text{NA}/n$. The theoretical intensity distribution in the back focal plane is shown in Fig. 2(c) for a source dipole located at $z_0 = 0$. For comparison with experimental data the calculated intensity distribution has been multiplied with $\cos\theta$ in order to account for the apodization of the collection objective. A cross section through the center of the field distribution is given in Fig. 2(d). The theoretical distributions are in good agreement with the experimental data shown in Figs. 2(a) and 2(b), which provides strong support for the “localized gap plasmon” hypothesis.

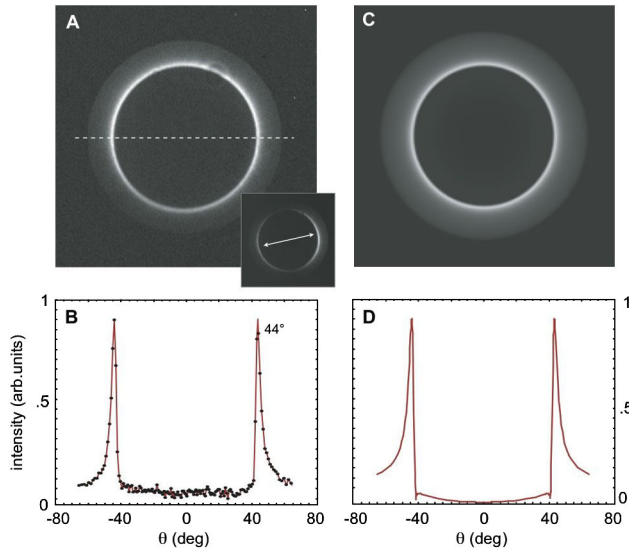


FIG. 2 (color online). Emission pattern (photon momentum distribution) measured in the back focal plane of the objective. Inelastically tunneling electrons couple to propagating SPPs which decay by leakage radiation. (a) Experimental back focal plane image for a 20 nm Au film showing a plasmon ring centered at $\theta \approx 44^\circ$. $V_t = 2.5$ V, $I_t = 1.5$ nA. Inset: Back focal plane image after passing through a polarizer oriented along the arrow in the figure. The extinction ratio is $>80\%$. (b) Cross section evaluated along the dashed line in (a). (c) Theoretical back focal plane image for $\lambda = 700$ nm according to Eq. (1). (d) Theoretical cross section through the center of (c).

To provide further evidence for the dipolelike character of the gap plasmon we record an optical image of the tunnel junction. This is accomplished by refocusing the fields in the back focal plane of the objective on a CCD. The resulting image corresponds to the Fourier transform of Eq. (1). If the dominant contribution to light emission does indeed originate from a vertical dipole, we expect an intensity null along the optical axis, which follows from symmetry considerations. In Fig. 3 we show both the experimental image [3(a)] and the theoretical image [3(b)] along with cross sections through the center of the patterns. In both images we indeed find an intensity minimum at the center enclosed by concentric interference rings. These rings originate from the interference of counterpropagating waves with well-defined k vectors (leakage radiation from SPPs) on the image screen. Because of background noise, surface roughness of the film, finite detector pixel size, and tip asymmetry, the minimum in the experimental image is not a perfect null. Nevertheless, the data agree well with theory and provide further support for the dipole nature of the gap plasmon.

The gap plasmon can be quenched by replacing the gold tip with a material that provides sufficiently high dissipation. To demonstrate this effect we repeated our experiments with a tungsten tip. As expected, the overall intensity of the emitted radiation dropped by more than 1 order of magnitude. The need for an Au-Au junction for enhanced light emission is further supported by the practice of “indenting” a tungsten tip in gold, as reported in previous studies [18,26].

For applications in nanophotonics it is desirable to have an electrically excited nanoscale photon source. For such a source to be practical, the electrical excitation region and the photon emission region need to be spatially separated, which is not the case for the extended gold film discussed

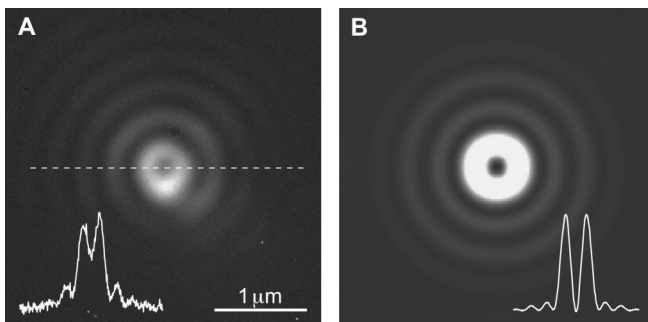


FIG. 3. Real-space images of the tunnel junction. (a) Experimental image and cross section recorded by refocusing the photons collected by the objective on a CCD. (b) Theoretical image corresponding to the square modulus of the Fourier transform of Eq. (1). The minimum at the center originates from the vertical dipole associated with the gap plasmon. The concentric interference rings indicate that the interfering fields have well-defined energy and momentum (leakage radiation from SPPs).

so far. However, the spatial separation of excitation and emission can be accomplished by exploiting plasmons in confined geometries, such as a gold nanowire. As illustrated in Fig. 1, we excite SPPs on one end of a nanowire by electron tunneling. Excited SPPs then propagate towards the other end where they are converted to propagating photons by scattering. Thus, the nanowire functions as a transmission line mediating between the electrical feed point and the optical outcoupling region.

The monocrystalline gold nanowires used in our experiments were synthesized by wet chemistry [27] and then dispersed on an indium tin oxide (ITO) coated glass substrate. The nanowire sample was then characterized by scanning electron microscopy (SEM) and by optical light scattering. To minimize SPP propagation losses and to improve the outcoupling efficiency, we selected individual wires with radii in the range of 50–100 nm [28]. Figure 4(a) shows a SEM image of a selected nanowire of radius 87 nm that has been cut to a length of $\sim 5 \mu\text{m}$ by focused ion beam milling [22]. Using a translation stage we positioned the nanowire into the field of view of the objective lens and placed the STM tip over one of the wire’s ends. Similar to the case of the planar gold film, electron tunneling gives rise to a gap plasmon, which can be described by an oscillating vertical dipole. The gap plasmon then couples to SPPs propagating along the gold nanowire, and once the SPPs reach the other end of the nanowire they are scattered and partially converted to free-propagating photons. Emitted photons are collected with the objective lens and then refocused on an image plane. In order to prevent propagating SPPs from decaying via leakage radiation [28], the nanowire sample has been covered with index matching oil [29].

Figure 4(b) shows the direct space photon map for the nanowire in Fig. 4(a). SPPs are excited by electron tunneling at the left end of the wire. The bias voltage is $V_t = 2 \text{ V}$ and the tunnel current $I_t = 1 \text{ nA}$. The map indicates that no photons are emitted along the nanowire and that a remarkable fraction of photons emerges from the wire ends. Similar results have been recorded for other wires as well. Because of the strong localization at the nanowire end, the field distribution in the back focal plane (Fourier plane) is very broad [22]. For the nanowire shown in Fig. 4, we measure $15\,000 \text{ photons s}^{-1}$ emitted from the tunnel junction whereas the total counts from the opposite end are $750 \text{ photons s}^{-1}$. Thus, the overall coupling efficiency along the nanowire is $\sim 5\%$. The efficiency improves for shorter nanowires because of lower propagation losses. Further improvement requires optimization of the coupling between gap plasmons and propagating SPPs and optimization of the SPP outcoupling on the opposite end of the nanowire.

The nanowire serves as a proof-of-principle geometry and is by no means an optimized configuration. Engineered plasmonic structures, such as optical antennas [30], will be

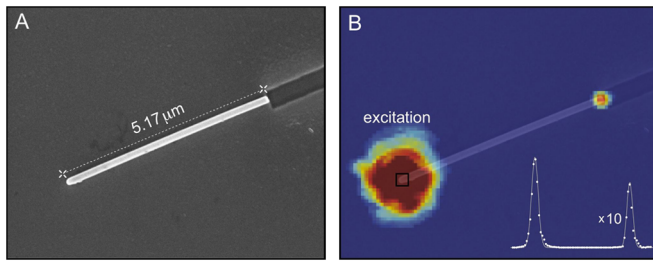


FIG. 4 (color online). Electrical excitation of SPPs propagating along a monocrystalline gold nanowire. (a) SEM image of a gold nanowire of radius 87 nm and length $\sim 5 \mu\text{m}$. (b) Photon emission map superimposed to the SEM image. SPPs excited at one end of the wire propagate to the other end where they are scattered and converted to propagating photons. Inset: Intensity map along the nanowire showing diffraction-limited emission peaks from both ends.

able to improve the electron-photon conversion efficiency. Because of the spatial separation of SPP excitation and SPP outcoupling, the optimization can proceed in two separate steps: the optimization of the tunneling junction and the optimization of the photon emission region. The former is a function of both the electronic and electromagnetic density of states whereas the latter constitutes a canonical antenna problem.

Our work demonstrates that low-energy electrons can couple to photons through a cascade of events. Tunneling electrons first excite gap plasmons, which in turn couple to propagating SPPs. The latter are then converted to photons via scattering. Thus, electron tunneling provides a non-optical, voltage-controlled, low-energy, and nanoscale pathway for launching SPPs in nanostructures. Our experiments were carried out under ambient conditions and do not require any vacuum conditions. It is important to point out the advantages of our technique over related schemes. While high-energy electrons provide a highly localized source for exciting plasmons, they are impractical for on-chip implementation. Also, exciton-mediated approaches using inorganic or organic semiconductors require multi-step fabrication which increases device complexity. The method introduced here, on the other hand, only demands metal electrodes that can be easily integrated in a planar geometry. Moreover, the low voltages required make it completely compatible with current complementary metal oxide semiconductor (CMOS) technology, thus enabling electron-photon signal transduction in integrated optoelectronic nanodevices.

This research was funded by the U.S. Department of Energy (Grant No. DE-FG02-01ER15204). A.B. thanks the NanoSci E+ program E²-PLAS (ANR-08-NSCI-007) for financial support. We thank Gustavo Cançado and Hayk Harutyunyan for valuable input and fruitful discussions.

Note added in proof.—A related study appeared recently in [31].

*<http://www.nano-optics.org>

- [1] F. J. G. de Abajo, *Rev. Mod. Phys.* **82**, 209 (2010).
- [2] R. H. Ritchie, *Phys. Rev.* **106**, 874 (1957).
- [3] M. V. Bashevoy *et al.*, *Nano Lett.* **6**, 1113 (2006).
- [4] E. J. R. Vesseur *et al.*, *Nano Lett.* **7**, 2843 (2007).
- [5] W. Cai *et al.*, *Nano Lett.* **9**, 1176 (2009).
- [6] J. Nelayah *et al.*, *Nature Phys.* **3**, 348 (2007).
- [7] M. Kuttge, E. J. R. Vesseur, and A. Polman, *Appl. Phys. Lett.* **94**, 183104 (2009).
- [8] J. Lambe and S. L. McCarthy, *Phys. Rev. Lett.* **37**, 923 (1976).
- [9] J. K. Gimzewski, B. Reihl, J. H. Coombs, and R. R. Schlittler, *Z. Phys. B* **72**, 497 (1988).
- [10] J. Coombs, J. Gimzewski, B. Reihl, and J. Sass, *J. Microsc.* **152**, 325 (1988).
- [11] P. Johansson, R. Monreal, and P. Apell, *Phys. Rev. B* **42**, 9210 (1990).
- [12] R. Berndt, J. K. Gimzewski, and P. Johansson, *Phys. Rev. Lett.* **67**, 3796 (1991).
- [13] Y. Uehara, Y. Kimura, S. Ushioda, and K. Takeuchi, *Jpn. J. Appl. Phys.* **31**, 2465 (1992).
- [14] S. Ushioda, Y. Uehara, and M. Kuwahara, *Appl. Surf. Sci.* **60-61**, 448 (1992).
- [15] K. Takeuchi, Y. Uehara, S. Ushioda, and S. Morita, *J. Vac. Sci. Technol. B* **9**, 557 (1991).
- [16] J. Aizpurua, G. Hoffmann, S. P. Apell, and R. Berndt, *Phys. Rev. Lett.* **89**, 156803 (2002).
- [17] Z. C. Dong *et al.*, *Phys. Rev. Lett.* **92**, 86801 (2004).
- [18] G. Schull, N. Néel, P. Johansson, and R. Berndt, *Phys. Rev. Lett.* **102**, 057401 (2009).
- [19] C. Chen, C. A. Bobisch, and W. Ho, *Science* **325**, 981 (2009).
- [20] R. J. Walters *et al.*, *Nature Mater.* **9**, 21 (2009).
- [21] D. M. Koller *et al.*, *Nat. Photon.* **2**, 684 (2008).
- [22] See supplemental material at <http://link.aps.org/supplemental/10.1103/PhysRevLett.106.226802> for photon emission spectra and nanowire characterization.
- [23] J. Aizpurua, S. P. Apell, and R. Berndt, *Phys. Rev. B* **62**, 2065 (2000).
- [24] M. A. Lieb, J. Zavislan, and L. Novotny, *J. Opt. Soc. Am. B* **21**, 1210 (2004).
- [25] L. Novotny and B. Hecht, *Principles of Nano-Optics* (Cambridge University Press, Cambridge, England, 2006).
- [26] G. Schull, M. Becker, and R. Berndt, *Phys. Rev. Lett.* **101**, 136801 (2008).
- [27] Z. Guo *et al.*, *Colloids Surf. A* **278**, 33 (2006).
- [28] T. Shegai *et al.*, *Nano Lett.* **11**, 706 (2011).
- [29] R. Pechou *et al.*, *Eur. Phys. J. Appl. Phys.* **2**, 135 (1998).
- [30] L. Novotny and N. F. van Hulst, *Nat. Photon.* **5**, 83 (2011).
- [31] T. Wang *et al.*, *Nanotechnology* **22**, 175201 (2011).

Supplementary Information

Electrical excitation of surface plasmons

Palash Bharadwaj¹, Alexandre Bouhelier² and Lukas Novotny^{1,3}

¹*Department of Physics and Astronomy, University of Rochester, Rochester, NY 14627, USA.*

²*Laboratoire Interdisciplinaire Carnot de Bourgogne, CNRS UMR-5209, Université de Bourgogne, 21000 Dijon, France.*

³*Institute of Optics, University of Rochester, Rochester, NY 14627, USA.*

Emission Spectra

Fig. S1 shows the spectrum of the photons emitted by the nanowire shown in Fig. 4 in the main text. The spectrum has been acquired for a bias of 2 V and a tunnel current of 1 nA. It features a peak at $\lambda \sim 720$ nm and extends into the near infrared. Similar spectra are seen for the case of continuous Au

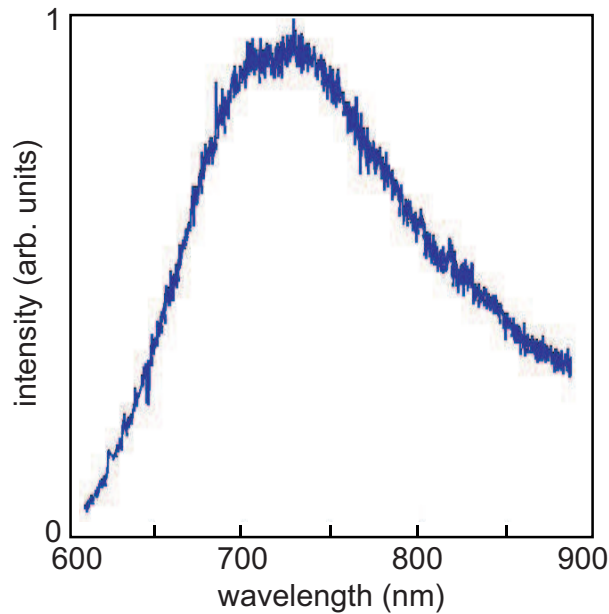


Figure S1: (a) Spectrum corresponding to the photon map shown in Fig. 4(b) in the main text.

film as well.

Fourier Plane Imaging of Nanowires

Fig. S2(a) is the backfocal plane image of the photons emitted by the nanowire shown in Fig. 4 in the main text. The backfocal plane image corresponds to the spatial spectrum, or Fourier transform, of the photon map shown in Fig. 4(b). The radius of the circle defined by the boundary between the bright disk and the black background corresponds to $\theta_{\max} \sim 68^\circ$, which is the maximum collection angle defined by the numerical aperture $NA = 1.4$ of the objective. Inside the circle of θ_{\max} the spatial spectrum is uniform and featureless, which indicates that the photons emerge from strongly localized regions, namely the ends of the nanowire.

The nanowire studied in the main text was immersed in oil. Fig. S2(b) shows results from a similar nanowire but without oil immersion. As before, the nanowire is excited by electron tunneling at one end of the nanowire, but this time the excited SPPs can decay via leakage radiation along the length of the nanowire. The line in the upper right of Fig. S2(b) indicates that the photons are localized in one dimension (transverse to nanowire axis) and delocalized in the other dimension (along the nanowire axis).

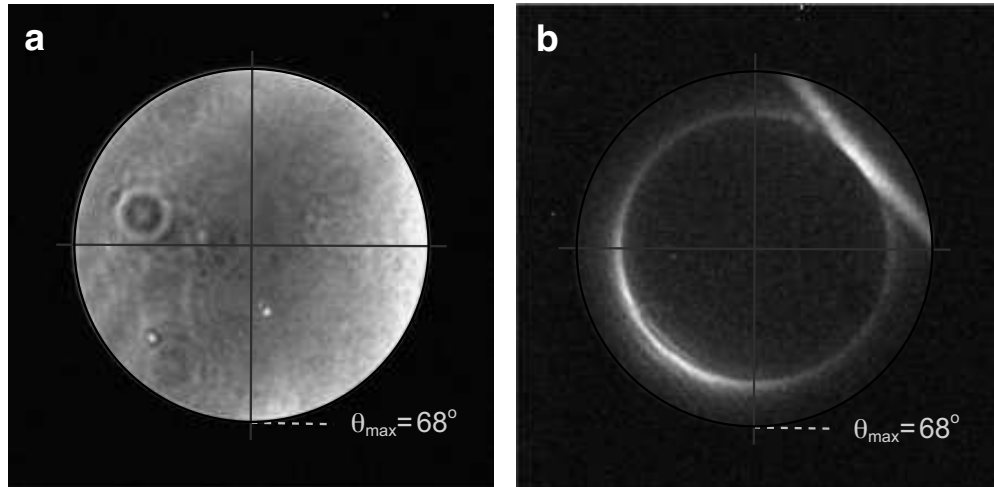


Figure S2: (a) Back focal plane image corresponding to the photon map shown in Fig. 4(b) in the main text. (b) Back focal plane image of photoemission from a different nanowire *without* oil immersion.

SEM Characterization of Nanowires

In Fig. S3 we show a sequence of scanning electron microscope (SEM) images of the monocrystalline gold nanowire used in the main text. These nanowires are formed as a by-product of synthesizing

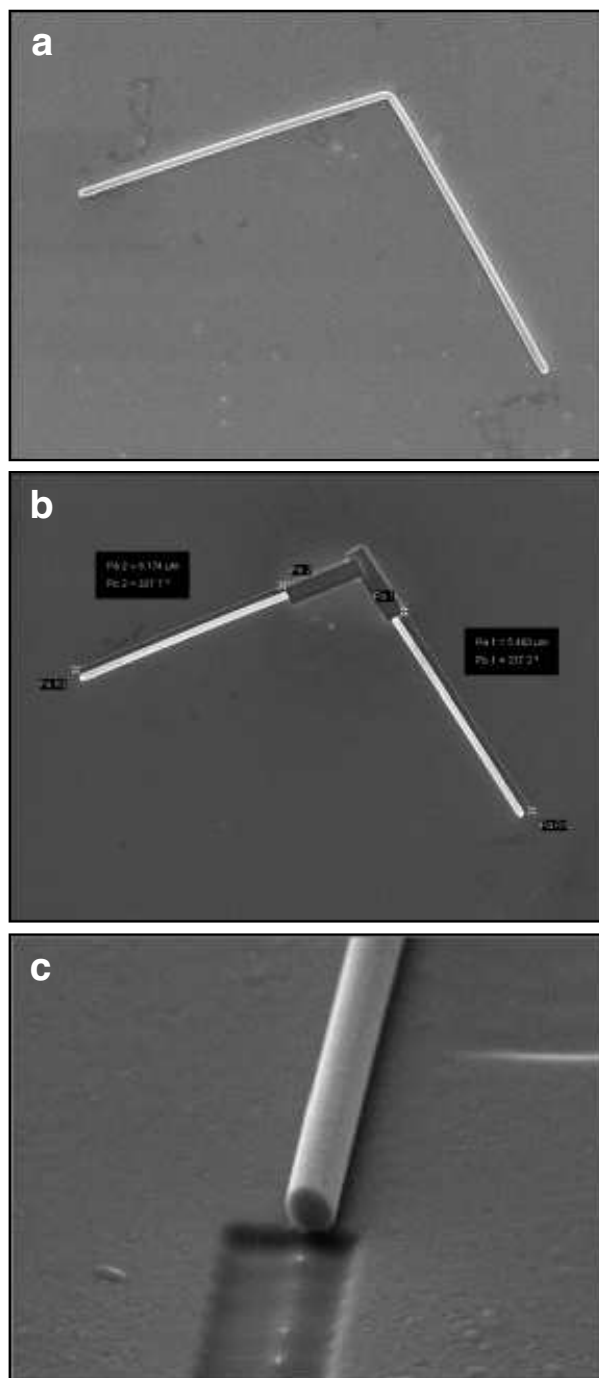


Figure S3: SEM images of the monocrystalline gold nanowire used in the main text.

monocrystalline Au flakes (using the recipe of Ref. 27 in main text). Fig. S3(a) shows the nanowire as deposited on the indium-tin-oxide (ITO) coated glass substrate. The wire features a kink that divides the wire into two segments of length $\sim 7\mu\text{m}$. Fig. S3(b) shows the nanowire after modification by focused ion beam (FIB) milling near the kink. FIB milling also partially removes the ITO coating. Fig. S3(c) shows a side view of the nanowire indicating a wire diameter of 87nm.